Seven-Helix Bundles:
Molecular Modeling via Restrained Molecular Dynamics

Mark S. P. Sansom, Hyeon S. Son, Ramasubbu Sankararamakrishnan, Ian D. Kerr, and Jason Breed

Laboratory of Molecular Biophysics, University of Oxford, Oxford, United Kingdom

ABSTRACT   Simulated annealing via restrained molecular dynamics (SA/MD) has been used to model compact bundles of seven approximately (anti)parallel α-helices. Seven such helix bundles occur, e.g., in bacteriorhodopsin, in rhodopsin, and in the channel-forming N-terminal domain of *Bacillus thuringiensis* δ-endotoxin. Two classes of model are considered: (a) those consisting of seven Ala_{20} peptide chains; and (b) those containing a single polypeptide chain, made up of seven Ala_{20} helices linked by Gly_N interhelix loops (where $N = 5$ or 10). Three different starting $C\alpha$ templates for SA/MD are used, in which the seven helices are arranged (a) on a left-handed circular template, (b) on a bacteriorhodopsin-like template, or (c) on a zig-zag template. The ensembles of models generated by SA/MD are analyzed in terms of their geometry and energetics, and the most stable structures from each ensemble are examined in greater detail. Structures resembling bacteriorhodopsin and structures resembling δ-endotoxin are both represented among the most stable structures. δ-Endotoxin-like structures arise from both circular and bacteriorhodopsin-like $C\alpha$ templates. A third helix-packing mode occurs several times among the stable structures, regardless of the $C\alpha$ template and of the presence or absence of interhelix loops. It is characterized by a "4+1" core, in which four helices form a distorted left-handed supercoil around a central, buried helix. The remaining two helices pack onto the outside of the core. This packing mode is comparable with that proposed for rhodopsin on the basis of two-dimensional electron crystallographic and sequence analysis studies.

INTRODUCTION

Several integral membrane proteins have been demonstrated to contain of bundles of transmembrane (TM) helices, e.g., bacteriorhodopsin (BR) (Henderson et al., 1990), photosynthetic reaction center (Deisenhofer et al., 1985), and light harvesting complex (Kühlbrandt and Wang, 1994). Furthermore, analysis of membrane protein sequences suggests that many, if not most, integral membrane proteins contain one or more TM helices. There is considerable evidence that TM helices act as independent folding domains that can self-assemble within lipid bilayers to form intact protein molecules (Popot and Engelman, 1990; Popot, 1993). For example, isolated helices of bacteriorhodopsin adopt their native secondary structure when in a membrane mimetic environment (Barsukov et al., 1992; Lomize et al., 1992; Pervushin and Arseniev, 1992), and functional BR molecules may be formed by self-assembly of proteolytic fragments (Kahn, 1992). Similarly, simple α-helical peptides can self-assemble within lipid bilayers to form transmembrane pores (Sansom, 1991, 1993). It is therefore of interest to attempt to model interactions within bundles of TM helices.

There is ongoing interest in the development of computational tools for modeling the structures of integral membrane proteins (Taylor et al., 1994). There are two reasons for believing that such an endeavor will prove successful: (a) the behavior of TM helices as independent folding domains; and (b) the restraints on possible modes of packing of TM helices imposed by the essentially two-dimensional nature of biological membranes. Considerable efforts have been expended to identify TM helices within the sequences of membrane proteins (von Heijne, 1992; Jones et al., 1994; Persson and Argos, 1994) and more recently to identify the internal and external faces of TM helices when present in bundles (Cronet et al., 1993; Donnelly et al., 1993; Tuffery et al., 1994). Fewer investigations have been made of the problem of modeling interactions between TM helices (Lemmon and Engelman, 1994). However, there is an extensive literature on helix packing interactions within soluble proteins (Chothia et al., 1981; Reddy and Blundell, 1993).

The seven transmembrane helix (7TM) bundle is a valuable test system for investigating helix packing within membrane proteins. The crystallographic structure of BR, the archetypal 7TM protein, has been determined at 3.4 Å resolution by electron diffraction (Henderson et al., 1990), providing detailed information on the geometry of helix packing. The 7TM bundle motif is also present in a large superfamily of G protein-coupled receptors (GPCRs), of which about 400 sequences are known (Donnelly and Findlay, 1994; Watson and Arkinstall, 1994). This superfamily includes rhodopsin, the two-dimensional projection structure, which has been determined at 9 Å resolution (Schertler et al., 1993). There have been several molecular modeling studies of 7TM bundles, ranging from homology modeling of GPCRs on the basis of the BR coordinates (Hibert et al., 1991; Livingstone et al., 1992; MaloneyHuss and Lybrand, 1992; Sylte et al., 1993) to energy minimization studies of the interactions of Ala_{14} helices within a 7TM bundle (Furois-Corbin and Pullman, 1986b). However, there have been fewer studies of the possible geometries of 7TM bundles

resulting from the stereochemistry of helix-helix inter-
actions (Chothia, 1984) plus the requirement for TM he-
lices to lie approximately (anti)parallel to one another and
to the bilayer normal.

In this paper, we undertake a systematic investigation of
possible structures for 7TM bundles. Ala_{20} is considered as
a simple model of a hydrophobic helix. The main aim of this
study is to determine how seven (anti)parallel hydrophobic
helices may pack together within a compact bundle. In par-
ticular, we investigate whether favored low energy structures
emerge as a result of simple helix packing considerations.
The computational procedure used is that of simulated an-
nealing via restrained molecular dynamics simulations (SA/
MD). This is similar to the method used successfully to pre-
dict the structure of a leucine zipper helix dimer (Nilges and
Brünger, 1991; Nilges and Brünger, 1993). SA/MD has been
used previously to model ion channels formed by symmetric
bundles of parallel TM helices (Kerr et al., 1994). This simu-
lation method provides a better sampling of conformational
space than, e.g., energy minimization based methods. Two
subsidiary aspects of this investigation are: (a) do inter-
helix loops result in perturbation of TM helix packing?; and
(b) how sensitive is TM helix packing to the initial $C\alpha$ co-
ordinates used in SA/MD? The question of sensitivity is of
evident importance if this technique is to be used to model
membrane proteins of unknown structure. Structures gener-
ated via simulations are compared with known experimental
structures for 7TM helix bundles.

MATERIALS AND METHODS

Programs

Molecular dynamics (MD) simulations and model building were carried out
using Xplor V3.1 (Brünger, 1992) with the CHARMM PARAM19 (Brooks
et al., 1983) parameter set. The latter was modified to increase the force
constant of the dihedral angle term used to maintain *trans* planar peptide
bonds. Only those H atoms attached to polar groups were represented ex-
plicitly, apolar groups being represented using extended atoms. Display and
examination of models was carried out using Quanta V4.0 (Molecular Simu-
lations), and diagrams of structures were drawn using Molscript (Kraulis,
1991). MD simulations were performed on a DEC 3000 400 computer. All
other calculations were carried out on a Silicon Graphics Indigo R3000
workstation.

Simulated annealing via molecular dynamics

The SA/MD method used was similar to that already described in the context
of modeling parallel bundles of TM helices (Kerr et al., 1994), so only details
specific to the current study are described.

In Stage 1 of SA/MD, $C\alpha$ templates were constructed. These defined the
initial positions of the $C\alpha$ atoms of the Ala_{20} helices and (where included)
of the Gly_N loops. For each model, five $C\alpha$ templates were generated, dif-
fering in the helix orientations within the bundle and (where present) in the
initial $C\alpha$ coordinates of Gly_N loops.

$C\alpha$ coordinates of the helices were generated using a rise/residue = 1.5
Å and 100° turn/residue. Helices were generated with their axes parallel (or
antiparallel) to the z axis, their centers in the xy plane, and with an interaxial
separation of 9.4 Å between adjacent helices. After generating helices in an
initial bundle geometry (see Results), each helix was subjected to a random
rotation (on {0°,360°}) about its axis, and to a random translation (on {−4.5
Å,+4.5 Å}) parallel to z.

$C\alpha$ template coordinates for Gly_N loops linking adjacent Ala_{20} helices
were generated as follows. N evenly spaced points along a vector linking
$C\alpha$:20 of helix i and $C\alpha$:1 of helix $i+1$ were calculated. Coordinates for each
$C\alpha$ atom of the loop were generated using a Gaussian distribution (SD =
1 Å) centered on the corresponding point on the vector.

The remaining backbone and side-chain atoms were superimposed on the
$C\alpha$ atoms of the corresponding residues. The $C\alpha$ atoms of the helices re-
mained fixed throughout Stage 1, whereas the loop $C\alpha$ atoms were unre-
strained. Annealing started at 1000 K, during which weights for covalent
terms were gradually increased. A repulsive van der Waals potential was
slowly introduced after an initial delay. Once the weights for these terms
reached their final values, the system was cooled from 1000 to 300 K in steps
of 10 K and 0.5 ps. During cooling, van der Waals radii were reduced to
80% of their standard values to enable atoms to pass by one another. Elec-
trostatic terms were *not* included during Stage 1. One structure was gen-
erated for each of the five $C\alpha$ templates for a given ensemble.

Structures from Stage 1 were each subjected to 5 MD runs (Stage 2),
resulting in an ensemble of $5 \times 5 = 25$ final structures. Initial velocities
were assigned corresponding to 500 K. Harmonic restraints were imposed
on $C\alpha$ atoms of the helices at the beginning of Stage 2 and were gradually
relaxed as the temperature was reduced from 500 to 300 K. Distance re-
straints were also introduced at this point (see next section). On reaching
300 K, a burst (generally 5 ps) of constant temperature dynamics was per-
formed, followed by 1000 steps of conjugate gradient energy minimization.
During the latter burst of dynamics and energy minimization, no positional
restraints were imposed on the positions of $C\alpha$ atoms, but distance restraints
were maintained. During Stage 2, electrostatic interactions were introduced
into the potential energy function. All atoms are assigned partial charges as
defined by the PARAM19 parameter set, and a distance-dependent dielectric
($\epsilon = r$) was used.

Distance restraints

Intra- and interhelix distance restraints were imposed during Stage 2. Bi-
harmonic or square-well restraining functions were used, depending on the
model under investigation (see below). Intra-helix restraints, used to main-
tain α-helical geometry, acted between the carbonyl O of residue $i+4$ and
the amide H of residue i.

Interhelix distances restraints were used to maintain adjacent helices in
an approximately (anti)parallel orientation and/or to maintain a compact
bundle of helices. Restraints acted between pairs of virtual atoms. Each
virtual atom was defined as the midpoint of a group of $C\alpha$ atoms. Details
of the restraints used are provided below (Results).

Analysis of structures

Geometric and energetic parameters characterizing helix-helix interactions
within bundles were analyzed. Helix crossing angles (Ω) were determined
as described by Chothia et al. (1981). Interhelix separations (R) were given
by the distance between the midpoints of the $C\alpha$ atoms of the helix. En-
semble averages of Ω and R were determined across all sequence adjacent
helix pairs within an ensemble. Helix-helix interaction energies were cal-
culated as

$$\Delta E = E_{TOT} - \left(\sum_{i}^{N} E_{Hi} \right),$$

where E_{TOT} is the potential energy of the intact bundle and E_{Hi} is the potential
energy of helix i in isolation. Buried accessible surface areas (ΔA_{HH}) were
evaluated in a similar fashion using a probe radius of 1.6 Å. For those models
containing interhelix loops, helix-loop interaction energies were calculated
as

$$\Delta E_{HL} = E_{TOT} - E_H - E_L,$$

where E_H is the total (intra- plus interhelix) energy of the α-helices and E_L
is the total (intra- plus interloop) energy of the interhelix loops.

In analyzing the secondary structure of Gly_N loops, the definitions in Quanta 4.0 (related to those of Sibanda et al., 199) were used. So, if (i, j) implies an $O_i \leftarrow HN_j$ H-bond, the possible secondary structure elements are: (a) a 3-turn, containing an $(i, i + 3)$ H-bond; (b) a 4-turn, containing an $(i, i + 4)$ H-bond; (c) a 5-turn, containing an $(i, i + 5)$ H-bond; (d) a β-strand, in which residues i and j are distant in the sequence and in which there are two H-bond bridges near i and j; (e) a β-bulge (as defined by Richardson et al., 1978); (f) an α-helix, containing two or more consecutive 4-turns; and (g) random coil.

RESULTS

Anti-parallel helix dimers

The principal aim of this investigation is to model possible structures for bundles of transmembrane (TM) helices. Such bundles are formed by a single polypeptide chain looping back and forth across a bilayer and, consequently, contain a number of antiparallel helix pairs. Having in earlier studies examined parallel dimers of hydrophobic helices (Kerr et al., 1994; Breed et al., 1995), it is informative, as a prelude to the main investigation, to characterize the interactions within *anti-parallel* helix dimers.

Ala_{20} helices were chosen as representative of hydrophobic TM helices to focus on packing interactions per se. To enable investigation of possible effects of interhelix loops, Ala_{20} helix dimers were generated both with and without intervening Gly_N sequences (Table 1). Glycine was selected to permit maximum conformational flexibility of a loop while retaining it as a "covalent restraint" on helix packing. In bacteriorhodopsin (BR) the shortest interhelix loop is 5 residues long, and the mean loop length is 10 residues. Thus, dimers with Gly_5 and with Gly_{10} loops were modeled. All model sequences were blocked at their N and C termini with acetyl and amide groups, respectively, to minimize electrostatic end effects.

All three dimer ensembles (AA, AG5A, and AG10A; Table 1) were generated using $C\alpha$ templates corresponding to exactly antiparallel helices ($\Omega = 180°$), with an interaxial separation of 9.4 Å. As described in Materials and Methods, random rotations about the helix axes and random translations parallel to z were imposed. During Stage 2 of SA/MD a single interhelix distance restraint was imposed. This acted between the geometric centers of the $C\alpha$ atoms of either helix. The biharmonic restraint function took the form:

$$E_{RESTRAINT} = \min\left[E_{MAX}, \frac{SRT}{2\sigma^2}\right](d - d_{TARGET})^2,$$

with $E_{MAX} = 50$ kcal/mol and $S = 2.5$. An asymmetric, biharmonic restraint was imposed to allow the helices to approach one another more closely but prevent them from drifting too far apart. This was achieved by setting $\sigma = 5.0$ Å for

$d < d_{TARGET}$ and $\sigma = 1.0$ Å for $d > d_{TARGET}$, where d is the distance between the centers of the two helices and $d_{TARGET} = 9.4$ Å is the target distance for the restraint.

Energetic properties of the three dimer ensembles were analyzed (Table 2). For all three ensembles, the helix-helix interaction energy is -25 to -35 kcal/mol. Of this, -5 to -10 kcal/mol is contributed by electrostatic interactions of the antiparallel helices, and about -23 kcal/mol by the van der Waals interactions. A rather greater contribution of electrostatic interactions to antiparallel dimer stability was suggested by the results of Furois-Corbin and Pullman (1986a) on antiparallel Ala_N dimers. The $\Delta E_{HH,VDW}$ for antiparallel dimers is the same as that obtained for parallel dimers of Ala_{20} (Breed et al., 1995). The buried accessible surface area is also about the same for all three antiparallel ensembles, and is again comparable with that (~ -780 Å^2) for parallel dimers. Thus, the presence or absence of Gly_N loops does not appear to alter the strength of helix-helix interactions, which is comparable with that observed in parallel dimers of Ala_{20}.

Turning to the geometric properties of the dimers (Table 3), for all three ensembles the distribution of crossing angles is quite broad, but with a mean of $\sim -175°$. This indicates a degree of left-handed super-coiling within the dimers. For parallel Ala_{20} dimers, a similarly broad distribution was observed (Breed et al., 1995). Presence or absence of Gly_N loops does not appear to perturb significantly either the geometry of helix packing or the secondary structure of the Ala_{20} domains.

If one considers simulated annealing as a means by which to sample the conformational space compatible with a given helix packing motif, it is valuable to consider the structural properties of the most stable members of an ensemble. Two criteria have been used to define the most stable structures of an ensemble: (a) the structure with the lowest total potential energy (E_{TOT}); and (b) the structure with the lowest helix-helix interaction energy (ΔE_{HH}). The structures thus defined are summarized in Table 4, and the lowest E_{TOT} members of ensembles AA and AG5A are depicted in Fig. 1.

It is evident that in the most stable dimers the degree of helix crossing is more pronounced. All six models thus defined have $\Omega \approx -160°$, which corresponds to Class 3–4 ridges-in-grooves helix packing, as defined by Chothia et al. (1981). The greater extent of helix-helix interactions in these low energy dimers is also reflected in smaller helix-helix separations and larger buried accessible surface areas than the averages for the corresponding ensembles. As for the ensembles, the presence or absence of interhelix loops does not seem to significantly effect helix-helix packing within the most stable dimers. Interestingly, selection of the most stable dimers also revealed more pronounced helix crossing in parallel Ala_{20} dimers (Breed et al., 1995).

7TM bundles: definition of models

To understand the dependence of structures of model 7TM helix bundles on the presence or absence of interhelix loops on the initial $C\alpha$ templates and on the nature of the interhelix

TABLE 1　Dimers: definition of models

Ensemble	Sequence
AA	$(Ac\text{-}Ala_{20}\text{-}NH_2)_2$
AG5A	$Ac\text{-}Ala_{20}\text{-}Gly_5\text{-}Ala_{20}\text{-}NH_2$
AG10A	$Ac\text{-}Ala_{20}\text{-}Gly_{10}\text{-}Ala_{20}\text{-}NH_2$

TABLE 2   Dimers: energetic analysis

Ensemble	E_{TOT} (kcal/mol)	E_{VDW} (kcal/mol)	E_{ES} (kcal/mol)	$\Delta E_{HH,VDW}$ (kcal/mol)	$\Delta E_{HH,ES}$ (kcal/mol)	ΔA_{HH} (Å²)
AA	−705 (6)	−145 (4)	−588 (4)	−25 (5)	−9 (6)	−812 (66)
AG5A	−764 (9)	−150 (6)	−646 (5)	−21 (4)	−5 (3)	−762 (45)
AG10A	−842 (8)	−162 (6)	−716 (5)	−20 (6)	−4 (2)	−744 (73)

Note: In this and subsequent tables, parameters are given as ensemble averages (SD). VDW = van der Waals; ES = electrostatic.

TABLE 3   Dimers: geometric analysis

Ensemble	Ω (°)	R (Å)	ϕ (°)	Ψ (°)
AA	−173 (12)	8.0 (0.7)	−65 (4)	−40 (6)
AG5A	−174 (13)	8.2 (0.6)	−65 (6)	−41 (6)
AG10A	−177 (14)	8.4 (0.6)	−65 (7)	−40 (7)

Note: ϕ and Ψ are given for the helical residues, i.e., excluding the interhelix loops.

TABLE 4   Low energy dimers: energetic and geometric analysis

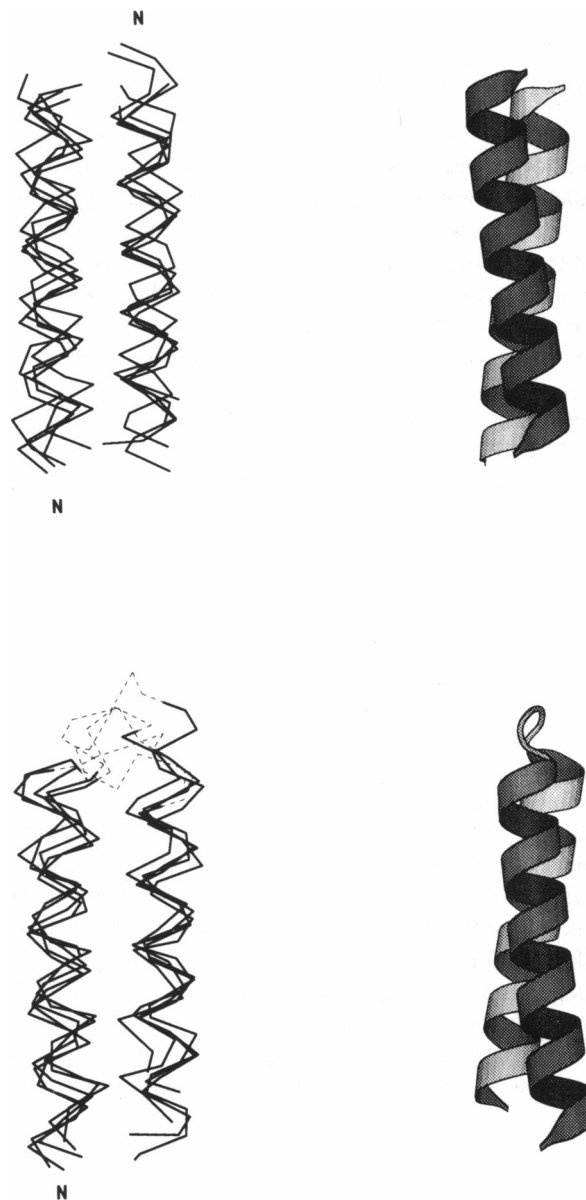| Structure	E_{TOT} (kcal/mol)	ΔE_{HH} (kcal/mol)	ΔA_{HH} (Å²)	Ω (°)	R (Å)
AA (3, 1)	−713	−38	−911	−166	7.9
AA (2, 5)	−711	−50	−830	−165	7.3
AG5A (1, 1)	−781	−29	−784	−164	7.8
AG5A (3, 2)	−769	−34	−804	−169	8.2
AG10A (4, 5)	−859	−27	−799	−171	8.1
AG10A (5, 4)	−834	−34	−814	−157	7.7

FIGURE 1   Anti-parallel helix dimers. Five structures selected at random from ensembles (A) AA and (B) AG5A are shown as superimposed Cα traces. The lowest E_{TOT} structures from these two ensembles are shown in B and D (structures AA(3,1) and AG5A(1,1), respectively) as ribbon plots drawn using MolScript (Kraulis, 1991).

distance restraints, multiple simulations were performed, as summarized in Table 5. Before discussing the results, it is informative to consider the rationale behind the choices of input parameters in these simulations.

As for the dimers, sequences with and without Gly_N loops (with $N = 5$ or 10) were investigated, and the N and C termini of the peptide chains were blocked with acetyl and amide groups, respectively. Each model used a Cα template in which alternate helices were antiparallel. Three classes of Cα template were used (Fig. 2): (a) a left-handed circle (as used by, e.g., Jähnig and Edhölm, 1992) in MD simulations of BR); (b) a BR-like triangular array, in which consecutive helices form two separate layers; and (c) a zig-zag triangular array, in which consecutive helices alternate between the two layers. Note that the latter two Cα templates correspond to two of the 5040 (=7!) possible arrangements of seven TM helices on the two-layered triangular lattice (Engelman et al., 1980). After placing the centers of the helices at the positions thus defined, initial randomization of the Cα templates was performed as described above.

Interhelix distance restraints differed between those models with and those without Gly_N loops. For those models *without* loops (i.e., ACH, ACS, ABH, and ABS), restraints were applied to (a) mimic the presence of interhelix loops and (b) maintain a compact bundle of approximately (anti)parallel helices. Loop restraints were applied between the appropriate terminal Cαs of adjacent pairs of helices (i.e., Cα:20 of helix 1 to Cα:1 of helix 2, etc.). The target distance for loop restraints was $d_{TARGET} = 12.7$ Å (obtained from

measurement of the corresponding distances in BR). Asymmetric restraints were used:- $\sigma = 10$ Å for $d < d_{TARGET}$, whereas $\sigma = 1.0$ Å for $d > d_{TARGET}$. Compactness of the bundle was maintained by restraining the distance between

TABLE 5 7TM bundles: definition of models

| Ensemble	Sequence	Cα template	restraints
ACH	(Ac-Ala$_{20}$-NH$_2$)$_7$	LH-circle	loops + compactness; biharmonic
ACS	(Ac-Ala$_{20}$-NH$_2$)$_7$	LH-circle	loops + compactness; square-well
ABH	(Ac-Ala$_{20}$-NH$_2$)$_7$	BR-like	loops + compactness; biharmonic
ABS	(Ac-Ala$_{20}$-NH$_2$)$_7$	BR-like	loops + compactness; square-well
AG5BH	Ac-(Ala$_{20}$-Gly$_5$)$_6$-Ala$_{20}$-NH$_2$	BR-like	compactness; biharmonic
AG5BS	Ac-(Ala$_{20}$-Gly$_5$)$_6$-Ala$_{20}$-NH$_2$	BR-like	compactness; square-well
AG5ZH	Ac-(Ala$_{20}$-Gly$_5$)$_6$-Ala$_{20}$-NH$_2$	zig-zag	compactness; biharmonic
AG10BH	Ac-(Ala$_{20}$-Gly$_{10}$)$_6$-Ala$_{20}$-NH$_2$	BR-like	compactness; biharmonic
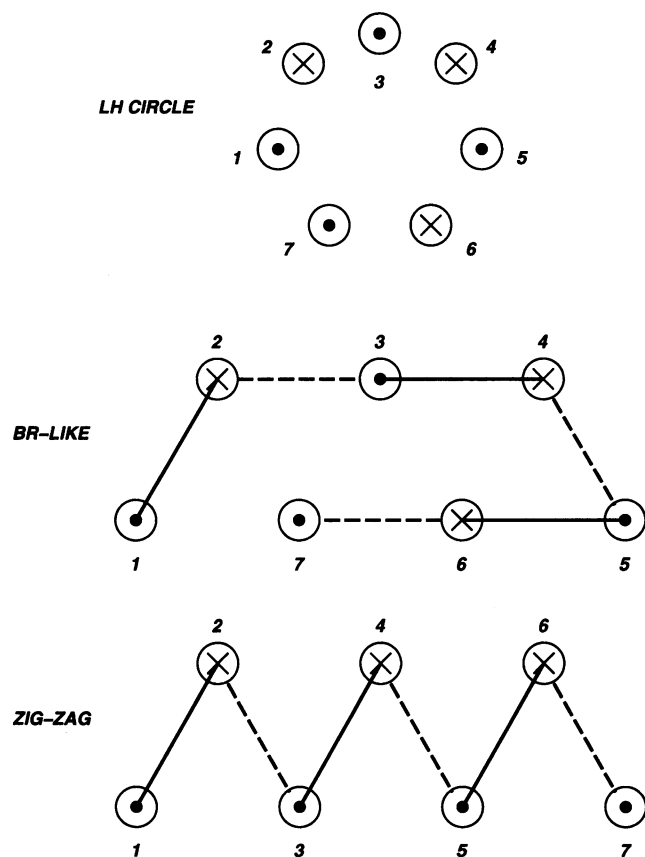
FIGURE 2   Schematic representations of the Cα templates used to generate 7TM helix bundles. (A) Left-handed circle template; (B) bacteriorhodopsin-like template; (C) zig-zag template. The circles represent helices. (●) C terminus of the helix toward the viewer; (×) N terminus toward the viewer. Solid and broken lines indicate the interhelix loops.

each helix i and the geometric center of the other six helices. Thus, a restraint was applied between helix 1 and the center of helices 2–7, etc. To maintain approximately (anti)parallel helices, such restraints were applied both between the midpoints of the helices and between their termini. Again, target distances were derived from the structure of BR. Thus, for the midpoints of the helices, $d_{\text{TARGET}} = 12.6$ Å, whereas for the termini $d_{\text{TARGET}} = 13.6$ Å. In both cases, $\sigma = 10$ Å for $d < d_{\text{TARGET}}$, whereas $\sigma = 1.0$ Å for $d > d_{\text{TARGET}}$. To characterize further the effects of loop and compactness restraints, two types of restraining function were investigated. In models ACH and ABH, a biharmonic restraint (as for the

dimers) was used. In models ACS and ABS, a square-well function was used:

$$E_{\text{RESTRAINT}} = \min[E_{\text{MAX}}, S] \, \Delta^2,$$

in which $\Delta = d - (d_{\text{TARGET}} - \sigma)$ for $d < d_{\text{TARGET}} - \sigma$, whereas $\Delta = d - (d_{\text{TARGET}} + \sigma)$ for $d > d_{\text{TARGET}} - \sigma$. For both types of restraining function, $E_{\text{MAX}} = 200$ kcal/mol and $S = 50$, resulting in firmer restraints than for the dimers. For models without interhelix loops the duration of the final MD burst of Stage 2 was 15 ps.

For models *with* Gly$_N$ loops (i.e., AG5BH, AG5BS, AG5ZH, and AG10BH), only compactness restraints were applied. These were applied only between the midpoints of the helices, and not between the termini. Other restraint parameters were as before, except that $E_{\text{MAX}} = 50$ kcal/mol and $S = 12.5$, resulting in softer restraints. The duration of the final MD burst of Stage 2 was 5 ps.

Examination of an ensemble of 7TM bundles

To assess the sampling of conformational space by SA/MD, one may examine chain traces of the 25 members of the ensemble (e.g., AG5BH, Fig. 3 A). Evidently, the imposed restraints permit considerable conformational variability. Such variability also reflects efficient sampling of conformational space by the simulation procedure. The columns of the array of structures in Fig. 3 A correspond to the five randomized Cα templates used (shown in the top row) and the rows to the Stage 2 runs. Note that there is no obvious clustering of structures within the ensemble corresponding to the Cα templates. Thus, as suggested by previous studies on parallel helix bundles, the Cα template is not the sole determinant of the final helix packing mode (Kerr et al., 1994). It is also important to note that although the helices retain their approximately (anti)parallel orientations, the centers of the helices do deviate from the positions defined by the initial template. This is particularly obvious for members (2,5) and (3,5) of the ensemble (where structure (i,j) was generated by Cα template i and MD (Stage 2) run number j), in which the "3+4" two-layered pattern of the BR-like template is absent from the final structure.

Within the conformational variability of the ensemble, statistical patterns emerge. From inspection of, e.g., structures (1,1), (1,5), and (2,3), it is evident that there is bias toward Ω values between $-170°$ and $-160°$. This is close to the ideal Class 3–4 ridges-in-grooves crossing angle of
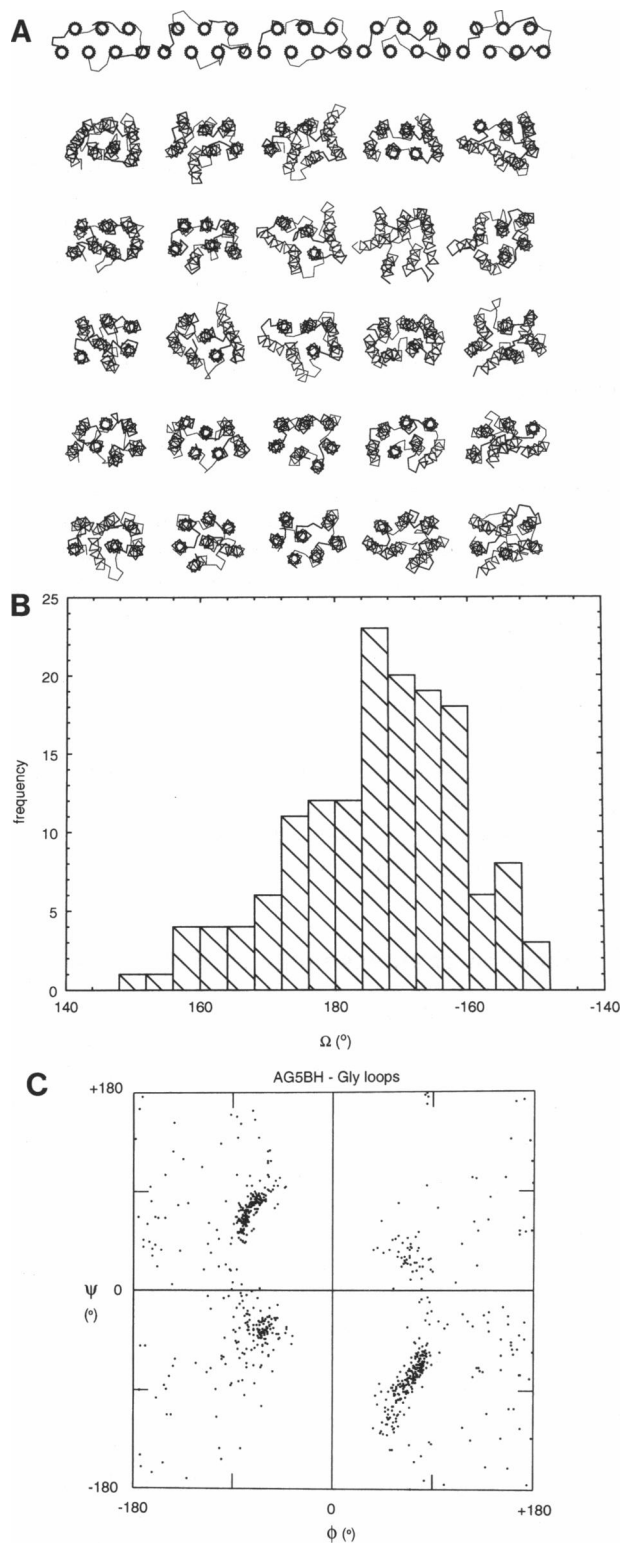
FIGURE 3   An ensemble of 7TM helix bundles. (A) All 25 members of ensemble AG5BH, shown as Cα traces. The top row of structures represents those generated by Stage 1, the remaining 5 rows showing the structures from each of the corresponding Stage 2 runs. In each structure, helix H1 is in the bottom left-hand corner and points up toward the viewer. (B) The distribution of helix crossing angles (Ω) between sequence adjacent antiparallel helix pairs for ensemble AG5BH. (C) Ramachandran plot of backbone (ϕ,ψ) angles for the interhelix loop Gly residues of ensemble AG5BH.

$\Omega = -160°$ (Chothia et al., 1981). This bias is confirmed by the distribution of Ω values between *sequence-adjacent* helices (i.e., helices i and $i+1$; Fig. 3 B). As expected for a conformationally diverse ensemble, this distribution is quite wide. However, the distribution is skewed with a mode of $\Omega \approx -170°$.

It is also of interest to examine briefly the Gly_5 loops within this ensemble. The secondary structures of interhelix loops are considered in more detail below. From the Cα traces (Fig. 3 A) it is evident that the loops adopt a number of different conformations. A Ramachandran plot for the loop residues (Fig. 3 C) shows the symmetry characteristic of glycine (ϕ,ψ) distributions (Richardson and Richardson, 1989).

7TM bundles: models without interhelix loops

Four ensembles of 7TM bundles lacking interhelix loops were investigated, as summarized in Table 5. For all four ensembles, the interaction energy per helix (Table 6) is $\Delta E_{HH}/7 \approx -30$ kcal/mol, i.e., comparable with that observed for helix dimers. Comparison of the energetics of AC ensembles with the AB ensembles reveals no significant differences between them either in total potential energy or in interaction energies. Thus, the nature of the Cα template (LH circle vs. BR-like) does not determine the energetics of helix packing within a bundle. This is supported by comparison of buried accessible surface areas. Comparison of those ensembles generated using a square-well restraining function (the S ensembles) with those generated using a biharmonic function (the H ensembles) suggests that the nature of the restraining function has a small effect on the energetics of helix packing. The S ensembles show, on average, somewhat stronger helix-helix interactions than the H ensembles.

Geometric properties of the bundles (Table 7) fail to reveal any major differences. In each ensemble, the (ϕ, ψ) values of the helices are close to observed values for proteins (Barlow and Thornton, 1988; Creighton, 1993). Helix-helix separations are somewhat greater for the H than for the S ensembles. Interestingly, mean interaxial distances between sequence adjacent helices are somewhat greater than for antiparallel helix dimers. To some extent, this reflects shuffling of the helices during Stage 2 such that those that are adjacent in the Cα template are not always adjacent in the final structure. Helix crossing angles for sequence-adjacent helices are divided into two groups for a 7TM bundle: those for antiparallel helix pairs (Ω_{AP}, i.e., Ω_{12} to Ω_{67}) and that for parallel helix pairs (Ω_{17}). Both groups of crossing angles show quite wide distributions, reflecting the conformational diversity within the ensembles. There is a bias toward Class 3–4 packing angles (for which $\Omega_{AP} \approx -160°$ and $\Omega_{17} \approx +20°$), but this is relatively small compared with the SDs of the crossing angle distributions.

Two low energy structures were selected from each ensemble, based on the those structures with the lowest values of E_{TOT} and of ΔE_{HH}. Energetic and geometric properties of the low energy bundles are summarized in Table 8. Inter-

action energies for these bundles are significantly lower than those of the parent ensembles. The Ω_{AP} and Ω_{17} values are consistent with Class 3–4 packing of adjacent helices, and the R values are smaller than for the parent ensembles. These observations confirm that these bundles reveal stable packing modes for 7TM bundles.

Similar modes are observed in low energy structures from different ensembles (Fig. 4). Thus, structures ACH(4,1), ACS(4,1), ABH(2,3) and ABH(1,2) all resemble the channel-forming domain of δ-endotoxin (δ-endoTx; Li et al., 1991), in which a central helix is surrounded by an outer

supercoil of six helices. Similarly, structures ACS(1,2), ABS(1,2) and ABS(4,4) all reveal a packing mode in which one helix (helix 4, 7, and 6, respectively) sits within a pocket formed by an arc of four tilted helices. This is reminiscent of the projection structure of rhodopsin (Rh) (Schertler et al., 1993). It is interesting that structure ACS(1,2), for which the template was an LH circle, exhibits the Rh-like packing mode, whereas ABH(2,3) and ACS(4,1) exhibit δ-endoTx-like packing modes, despite originating from different templates. This suggests that both templates allow access to the same energy minima.

Schematic representations of the packing modes of the low energy structures are shown in Fig. 5. A helix-helix contact may be defined as occurring when the midpoints of two helices lie within 12 Å of one another. (This somewhat relaxed definition takes into account increases in the separation of the midpoints as a result of displacement of helices relative to one another along z.) Structures ACH(4,1) and ACH(4,4) are relatively open, whereas in all other structures at least one helix forms contacts with ≥3 others. Comparison of the patterns of helix contacts with the ΔE_{HH} values reveals that, as anticipated, the more compact structures (defined by a greater number of contacts) are more stable. Helix contacts are formed between parallel helices as well as between antiparallel pairs. This is particularly evident in the δ-endoTx-like structures and suggests that the requirement for close helix packing overcomes unfavorable dipole interactions (Hol et al., 1981).

7TM bundles: models with interhelix loops

Four ensembles with interhelix loops were generated (Table 5). For Gly_5 loops and BR-like $C\alpha$ templates, both biharmonic and square-well restraining functions were investigated. For the models without loops, use of a square-well restraining function appeared to result in tighter helix packing. However, for models with loops, the opposite was the case (see below), and so biharmonic potentials were used for the other two ensembles, which used a zig-zag $C\alpha$ template and Gly_{10} loops, respectively.

Analysis of the energetics of the ensembles (Table 6) suggests that the strength of helix packing interactions does not differ much between the various ensembles with Gly_N loops. Averaging the helix interaction energy over all models with loops yields $\Delta E_{HH,VDW} \approx -150$ kcal/mol compared with $\Delta E_{HH,VDW} \approx -170$ kcal/mol for models without loops. A similar difference is observed in the $\Delta E_{HH,ES}$ values. Thus, helix-helix interactions are slightly weaker in ensembles with interhelix loops. However, the total E_{ES} is greater for those models with loops, reflecting formation of H-bonds from the loops to otherwise unsatisfied H-bond donors and acceptors at helix termini.

Geometrical analysis of the ensembles confirmed that mean (ϕ,ψ) values for the helices are unperturbed by the presence of Gly_N loops. The conformations of the loops are quite variable and are discussed in more detail below. As with the previous 7TM bundles, the interaxial distances are
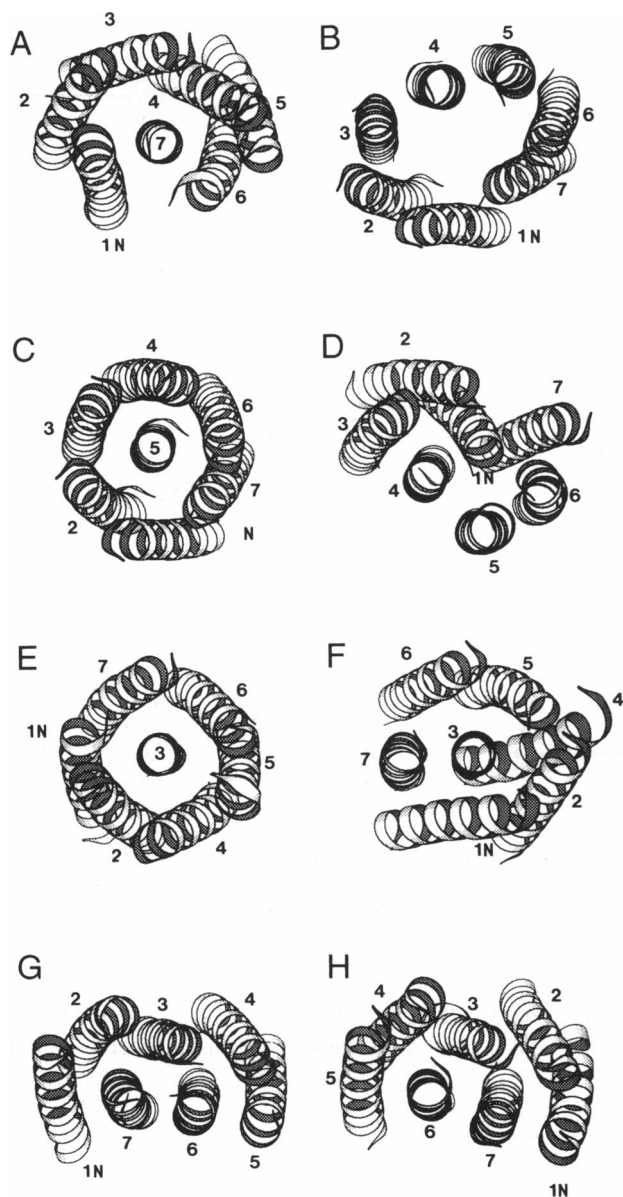
FIGURE 4   Low energy structures for 7TM helix bundles without interhelix loops. The structures shown are for ensembles ACH (A, ACH(4,1), lowest E_{TOT} and ΔE_{HH}; B, ACH(4,4), next lowest E_{TOT}); ACS (C) ACS(4,1), lowest E_{TOT}; D, ACS(1,2), lowest ΔE_{HH}); ABH (E, ABH(2,3), lowest E_{TOT} and ΔE_{HH}; F, ABH(1,2), next lowest E_{TOT}); and ABS (G, ABS(1,2), lowest E_{TOT}; H, ABS(4,4), lowest ΔE_{HH}). The positions of the seven helices, and of the N terminus of helix 1 are labeled.
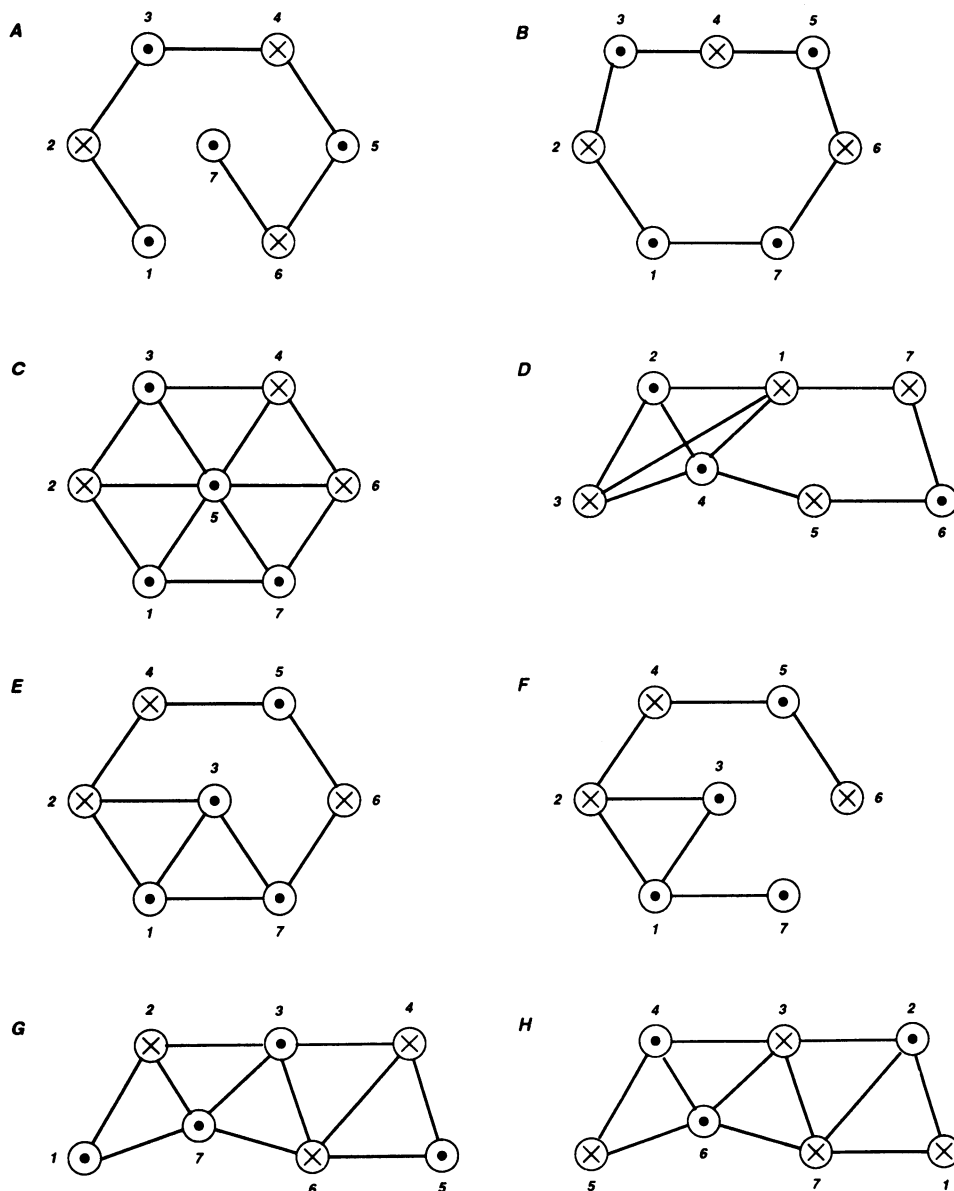
FIGURE 5 Schematic representations of the helix packing modes of the low energy structures for 7TM helix bundles without interhelix loops. The diagrams are for the structures shown in Fig. 4. (A) ACH(4,1); (B) ACH-(4,4); (C) ACS(4,1); (D) ACS(1,2); (E) ABH(2,3); (F) ABH(1,2); (G) ABS(1,2); and (H) ABS(4,4). Circles represent helices. (●) C terminus of the helix toward the viewer; (×) N terminus toward the viewer. (——) Helix-helix contacts, defined by the geometric centers of the helices approaching within 12 Å of one another.

somewhat greater than in helix dimers. The range of Ω values is quite wide, reflecting conformational diversity within the ensembles. Again, the mean Ω values reveal a small bias toward Class 3–4 packing of helices. Overall, analyses of both energetics and geometry fail to reveal any major differences in helix packing determined by the presence or absence of interhelix Gly_N loops.

As before, two low energy structures were defined for each ensemble (Fig. 6). These reveal a pronounced conservation of helix packing modes. For example, in models AG5BH-(1,1) and AG10BH(3,3) helices 1, 2, 3, and 6 form a left-handed arc around helix 7. This pattern is also found, despite the different $C\alpha$ template, in AG5ZH(1,4), in which helices 1, 2, 4, and 5 form a left-handed arc around helix 3. In all

TABLE 6   7TM bundles: energetic analysis

Ensemble	E_{TOT} (kcal/mol)	E_{VDW} (kcal/mol)	E_{ES} (kcal/mol)	$\Delta E_{HH,VDW}$ (kcal/mol)	$\Delta E_{HH,ES}$ (kcal/mol)	ΔA_{HH} (Å^2)
ACH	−2489 (15)	−600 (17)	−1990 (7)	−142 (16)	−39 (5)	−5300 (220)
ACS	−2584 (15)	−588 (11)	−2100 (7)	−187 (10)	−45 (6)	−6260 (170)
ABH	−2492 (14)	−612 (13)	−1980 (6)	−160 (14)	−29 (5)	−5680 (300)
ABS	−2594 (14)	−601 (8)	−2098 (10)	−199 (8)	−40 (8)	−6280 (100)
AG5BH	−2890 (18)	−662 (16)	−2356 (13)	−154 (17)	−23 (7)	−5852 (256)
AG5BS	−2904 (18)	−534 (15)	−2456 (14)	−126 (12)	−20 (5)	−5246 (242)
AG5ZH	−2898 (19)	−675 (13)	−2353 (11)	−158 (16)	−16 (4)	−5940 (272)
AG10BH	−3368 (27)	−744 (27)	−2778 (13)	−154 (20)	−23 (5)	−5840 (261)

TABLE 7   7TM bundles: geometric analysis

Ensemble	Ω_{AP} (°)	Ω_{17} (°)	R (Å)	ϕ (°)	Ψ (°)
ACH	−173 (9)	+9 (6)	9.0 (1.1)	−66 (5)	−39 (7)
ACS	−176 (15)	−5 (21)	8.6 (1.0)	−65 (6)	−41 (6)
ABH	−178 (19)	+4 (17)	9.6 (1.6)	−66 (7)	−39 (7)
ABS	−170 (8)	+11 (12)	8.9 (1.1)	−65 (5)	−40 (6)
AG5BH	−169 (6)	+4 (18)	9.0 (1.1)	−65 (8)	−40 (8)
AG5BS	−177 (18)	+11 (35)	9.2 (1.5)	−64 (8)	−42 (8)
AG5ZH	−174 (11)		9.8 (1.6)	−65 (10)	−40 (9)
AG10BH	−175 (14)	+11 (18)	8.9 (1.1)	−65 (9)	−40 (9)

Note: ϕ and Ψ are given for the helical residues, i.e., excluding the inter-helix loops.

three structures, the remaining two helices tilt to form part of an outer bundle around the five helix core.

The mean interaction energy for the low energy structures is −195 kcal/mol, compared with −169 kcal/mol for the parent ensembles. The Ω_{AP} and Ω_{17} values both reveal a greater tendency toward Class 3–4 helix packing than in the ensembles as a whole. These two observations confirm that these structures are more stable than the averages of the parent ensembles.

Comparison with experimental structures

The aim of this study is to simulate the packing of seven consecutive antiparallel helices within a compact bundle. Two experimentally determined structures satisfy this condition: bacteriorhodopsin (Henderson et al., 1990) and the N-terminal domain of *B. thuringiensis* δ-endotoxin (Li et al., 1991). BR is the archetypal integral membrane protein. δ-EndoTx, although a domain from a water-soluble protein, interacts with cell membranes to form ion-permeable pores, and during this process one or more of the seven helices insert into the lipid bilayer.

One of the low energy 7TM bundles, ACH(4,4) resembles the BR fold (Fig. 7, *A* and *B*). Both BR and ACH(4,4) contain a two-layered 3+4 helix bundle. In the 3-helix layer, the helices are approximately parallel to z, whereas the 4 helices of the other layer are tilted relative to z so as to form an arc of distorted left-handed supercoil. Both structures have Ω_{AP} ~−170° and Ω_{17} ~+10°, consistent with Class 3–4 ridges-in-grooves helix packing. The mean interaxial distance is greater in BR than in ACH(4,4). This is expected given the presence in BR of side chains larger than Ala.

There are some differences between helix packing in the two structures. In BR the 3-helix layer contains helices 2, 3, and 4, whereas the 4-helix layer contains helices 5, 6, 7, and 1 (counting in a clockwise direction with the C terminus of helix 1 pointing upwards). In ACH(4,4), the 3-helix layer contains helices 3, 4, and 5 and the 4-helix layer contains helices 6, 7, 1, and 2. Thus, the position of the parallel helix pair (1–7) within the two-layered bundle differs between the two structures. ACH(4,4) also has a somewhat larger central cavity than BR because the model bundle is less flattened than the experimental structure.

Two of the low energy bundles, ACS(4,1) and ABH(2,3), strongly resemble δ-endoTx in their helix packing, and an-

other two bundles, ACH(4,1) and ABH(1,2), provide distorted variants of the same fold. All contain the basic δ-endoTx-like 6+1 helix bundle, with an outer left-handed supercoil of 6 helices surrounding a central helix running approximately parallel to z (Fig. 7, *C* and *D*). Helix crossing angles (Ω_{AP} = −161°, −164° and −160° and Ω_{17} = +29°, +19°, and +22° for δ-endoTx, ACS(4,1) and ABH(2,3), respectively) are very close to the ideal values for Class 3–4 ridges-in-grooves packing. As with BR, the non-Ala side chains of δ-endoTx result in a greater interaxial separation than in the Ala_{20} bundles.

Differences between helix packing in δ-endoTx and in ACS(4,1) and ABH(2,3) reside in which helices run parallel to z and which run antiparallel. Thus, in δ-endoTx the outer ring is made up of helices 1, 7, 6, 4, 3, and 2 (counting clockwise with helix 1 pointing upwards). Helix 5 is in the center, pointing upwards (Fig. 7 *C*). In ACS(4,1) the outer ring is helices 1, 2, 3, 4, 6, 7, with 5 in the center pointing upwards; in ABH(2,3) the outer ring is 1, 2, 4, 5, 6, 7, with 3 in the center pointing upwards. However, in all three structures, there is a central layer of three parallel helices (helices 3, 5, and 7 in δ-endoTX; 3, 5, and 7 in ACS(4,1); and 1, 3, and 5 in ABH(2,3)). Thus, all three bundles contain four parallel pairwise helix interactions and eight antiparallel, rather than the three parallel and nine antiparallel that one might predict on the basis of optimization of helix dipole interactions (e.g., a ring of helices 1, 2, 3, 4, 5, and 6 with 7 in the center). This suggests that helix dipole interactions do not dominate such packing modes provided that optimal stereochemical criteria (i.e., helix crossing angles) are satisfied.

A conserved packing mode?

One packing mode is observed in several of the low energy structure: in ABS(1,2), ABS(4,4), AG5BH(1,1), AG5ZH-(1,4), AG10BH(3,3) and, in a distorted form, in ACS(1,2) and AG5BS(1,4). It is significant that this mode has been observed for different Cα templates (LH-circle, BR-like or zig-zag) and with or without Gly_N loops. This mode is characterized by a core structure of four helices forming an incomplete left-handed supercoil around a central helix approximately parallel to z, with another two helices packed onto the core. Overall, this mode satisfies the requirements of Class 3–4 ridges-in-grooves helix packing. Thus, Ω_{AP} = −166°, −163°, −169°, −161°, and −169° for ABS(1,2), ABS(4,4), AG5BH(1,1), AG5ZH(1,4), and AG10BH(3,3), respectively. This mode is also particularly stable; using ΔE_{HH} as a criterion, structures ABS(1,2) and ABS(4,4) are the most stable of those without Gly_N loops, and AG5ZH(1,4) and AG10BH(3,3) are the most stable of those with loops.

If one superimposes the helix axis vectors of ABS(1,2), AG5BH(1,1), AG5ZH(1,4), and AG10BH(3,3), the agreement is striking (Fig. 8 *B*), despite the reversed polarity of two of the helices in AG5ZH(1,4). The stability of the latter structure again argues for the precedence of stereochemical interactions over helix dipole interactions in determining sta-

TABLE 8 Low energy 7TM bundles: energetic and geometric analysis

Structure	Figs. 4 and 6	E_{TOT} (kcal/mol)	ΔE_{HH} (kcal/mol)	ΔA_{HH} (Å²)	Ω_{AP} (°)	Ω_{17} (°)	R (Å)
ACH (4, 1)	A	−2524	−217	−5907	−161 (5)	+19	8.7 (0.5)
ACH (4, 4)	B	−2506	−190	−5368	−170 (12)	+8	8.2 (0.2)
ACS (4, 1)	C	−2614	−242	−6519	−164 (4)	+19	8.4 (1.1)
ACS (1, 2)	D	−2609	−253	−6528	−170 (13)	−25	8.4 (0.6)
ABH (2, 3)	E	−2525	−213	−6111	−160 (5)	+22	10.0 (1.9)
ABH (1, 2)	F	−2514	−209	−6174	+162 (30)	−32	10.8 (2.3)
ABS (1, 2)	G	−2627	−266	−6421	−166 (3)	+19	8.5 (0.7)
ABS (4, 4)	H	−2615	−269	−6405	−163 (2)	+18	8.3 (0.3)
AG5BH (3, 1)	A	−2926	−190	−5969	−172 (16)	−21	8.5 (0.9)
AG5BH (1, 1)	B	−2880	−206	−5830	−169 (6)	+9	9.7 (1.5)
AG5BS (1, 4)	C	−2946	−162	−5761	−179 (13)	+25	10.2 (2.0)
AG5BS (1, 1)	D	−2923	−172	−5727	+170 (17)	+40	9.4 (1.2)
AG5ZH (4, 4)	E	−2941	−199	−6197	−171 (9)		9.8 (2.0)
AG5ZH (1, 4)	F	−2928	−214	−6164	−161 (3)		8.6 (1.0)
AG10BH (2, 5)	G	−3409	−194	−5944	−176 (14)	+11	9.5 (1.7)
AG10BH (3, 3)	H	−3400	−222	−6016	−163 (2)	+19	8.6 (0.9)
BR					−172 (11)	+9	10.7 (1.4)
δ-EndoTx					−161 (6)	+29	13.1 (2.6)

Note: The second column indicates the illustration of the structure in Fig. 4 or Fig. 6.

bility of bundles of simple hydrophobic helices. The agreement between the helix vectors is also significant given the differences in Cα templates, presence or absence of loops, and length of loops. Taken together, this suggests that this helix packing mode is stereochemically favored for 7TM helices.

This packing mode is similar to that observed in the 9 Å resolution projection structure of bovine Rh (Fig. 8 *A*) (Schertler et al., 1993). The Rh structure may be interpreted as ring of four helices surrounding a central helix, with the remaining two helices packing on the outside of the ring. It will be of considerable interest to examine how the stable packing mode for simple TM helices observed in simulation studies compares with the three dimensional arrangement of the helices in rhodopsin once the latter structure is reported (Unger and Schertler, 1994).

It is perhaps informative to speculate on the two conspicuous stable packing modes observed in the simulations: the δ-endoTx-like and Rh-like modes. Both provide solutions to the problem of how to pack 7 TM helices with optimal helix crossing angles and without a central cavity. The δ-endoTx-like structure may be classified as a 6+1 bundle. The core of the Rh-like structure may be classified as a 4+1 bundle. Structures that can be classified as 5+1 bundles are also found (e.g., ACH(4,1); Fig. 4 *A*). A 5+1 bundle may provide a stable packing mode for six helices and, thus, is of interest with respect to those integral membrane proteins, e.g., the ABC transporters (Higgins, 1993), which are believed to contain two 6TM helix domains.

Secondary structure of Gly$_N$ loops

What of the Gly$_N$ loops generated by SA/MD? So far, they have been considered as covalent restraints between adjacent helices, but one should also examine their conformations per

se. A Ramachandran plot for the Gly$_5$ loops of ensemble AG5BH (Fig. 3 *C*) is representative of (ϕ,ψ) distributions for the other loop-containing ensembles. In agreement with studies of Gly conformations in high resolution protein structures (Richardson and Richardson, 1989) both the α_R and α_L regions are significantly populated. The other highly populated regions ($\sim -90°, +90°$ and $\sim +90°, -90°$) are allowed regions (Creighton, 1993), although they are not generally occupied by Gly residues in protein structures. This difference may reflect the presence of multiple, consecutive Gly residues in the interhelix loops.

Visual inspection of loop-containing structures (Figs. 1 *B*, 3 *A*, and 6) reveals considerable conformational variability in the loops. Statistical analysis of their secondary structures (Table 9) reveals some consistent patterns. In all ensembles, both of dimers and of 7TM bundles, about 40% of the glycines adopt a random coil conformation. Of the remaining 60%, the majority adopt 3-turn, 5-turn, and α-helical conformations. H-bonded β-strand and β-bulge regions are relatively infrequent. Comparison of dimers and 7TM bundles reveals no significant differences in the secondary structure distributions of the interhelix loops.

Within the 7TM bundles, changing the nature of the restraining function (AG5BH vs. AG5BS) or changing the Cα template (AG5BH vs. AG5ZH) has no effect on the distribution of glycine conformations. However, increasing the length of the loops (AG5BH vs. AG10BH) results in a decrease in the percentage of α-helical glycines and an increase in the percentage of β-strands and β-bulges, reflecting greater opportunity for intra- and interloop H-bonding with Gly$_{10}$ loops. This pattern is also observed in the corresponding dimers.

Overall, the distribution of glycine secondary structures suggests that generation of interhelix loops from random starting coordinates using SA/MD is an effective minimal approach in the absence of experimental information on loop
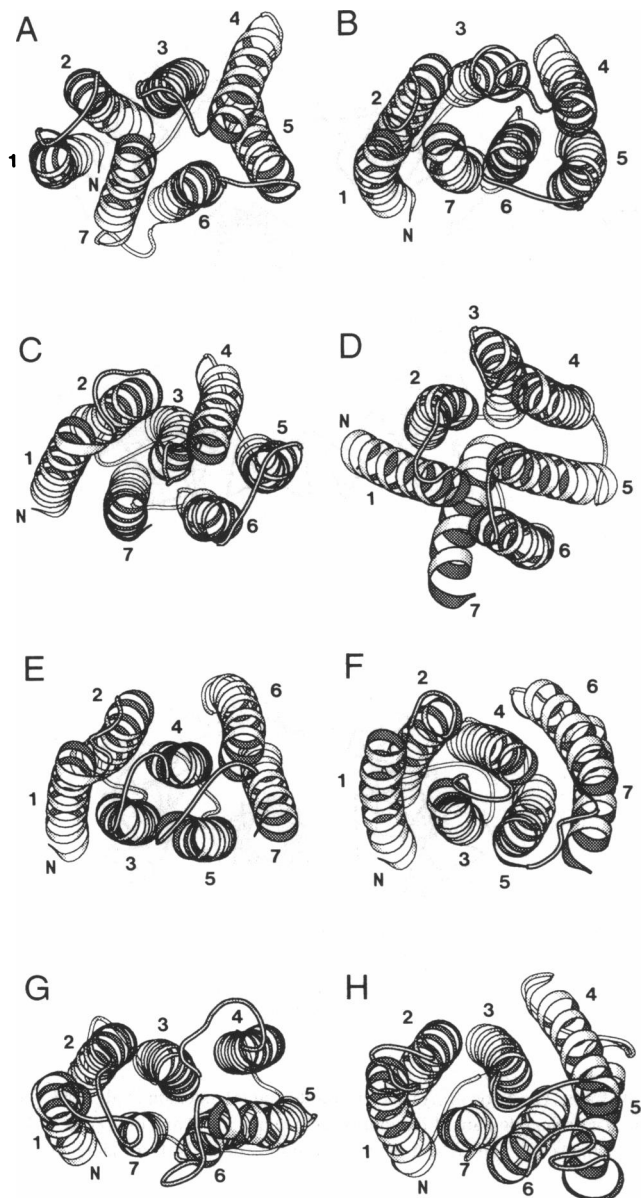
FIGURE 6 Low energy structures for 7TM helix bundles with interhelix Gly loops. The structures shown are for ensembles AG5BH (A, AG5BH-(3,1), lowest E_{TOT}; B, AG5BH(1,1), lowest ΔE_{HH}); AG5BS (C, AG5BS(1, 4), lowest E_{TOT}; D, AG5BS(1,1), lowest ΔE_{HH}); AG5ZH(E, AG5ZH(4,4), lowest E_{TOT}; F, AG5ZH(1,4), lowest ΔE_{HH}); and AG10BH (G, AG10BH-(2,5), lowest E_{TOT}; H, AG10BH(3,3), lowest ΔE_{HH}). The positions of the seven helices and of the N terminus of helix 1 are labeled.

conformations. One should remember that absence of explicit solvent molecules from these simulations may have an effect on possible loop conformations.

Helix-loop interactions

As discussed above, although helix-helix interactions are slightly weaker in bundles with interhelix loops than in those without, the overall electrostatic energy (E_{ES}) of the loop-containing bundles is greater. Visual inspection of the struc-

tures suggests this is a result of H-bonds formed from the loops to the termini of the helices. This may be quantified via evaluation of helix-loop interaction energies (ΔE_{HL}; Table 10). For dimers and for 7TM bundles, $\Delta E_{HL} \sim 2.5 \Delta E_{HH}$. Thus, the helix-loop interactions make a greater net contribution to bundle stabilization than do the helix-helix interactions. Of course, the most stable structures are those that optimize both helix-loop and helix-helix interactions. Furthermore, whereas helix-helix interactions are dominated by van der Waals interactions ($\Delta E_{HH,VDW}$; Tables 2 and 7), helix-loop interactions are predominantly electrostatic in origin ($\Delta E_{HL,ES}$; Table 10). As might be anticipated, helix-loop interactions are somewhat stronger when the loop length is extended from 5 to 10 residues.

DISCUSSION

Evaluation of methodology

Before considering the simulation results, it is necessary to evaluate the computational methodology. In support of SA/MD is its use to predict accurately the structure of the GCN4 Leu zipper helix dimer (Nilges and Brünger, 1991, 1993). SA/MD has also been used to model dimerization of glycophorin TM helices (Treutlein et al., 1992) and to analyze a helix dimerization motif present in this and related TM domains (Lemmon et al., 1994). More recently, SA/MD has been applied to ion channels formed by parallel bundles of TM helices (Kerr et al., 1994) and has aided in modeling effects of α-aminoisobutyric acid (Aib) residues on helix-helix interactions (Breed et al., 1995).

SA/MD possesses some advantages over related modeling techniques such as extended MD simulations at constant temperature or energy minimization-based conformational searches. Generation of an ensemble of structures by SA/MD is equivalent to many short MD simulations from different starting points. This enables a wider region of conformational space to be explored than would be the case for a single MD simulation of length equal to the sum of the SA/MD simulations (generally 25 ps).

An important aspect of analysis of SA/MD-generated structures is measurement of variations in geometrical and energetic parameters within an ensemble. Such variations should not be viewed as failure to converge, but rather as an indication of the range of structures compatible with the imposed restraints. Subsequent selection of the most stable structure and/or the structure with the strongest helix-helix interactions provides a way of filtering the variation within an ensemble.

To what extent are the structures generated by SA/MD determined by the interhelix restraints and Cα templates used? Our results suggest that the same stable 7TM packing modes (δ-endoTx-like and Rh-like) are observed for different restraining functions and for different Cα templates. SA/MD studies of alamethicin helix bundles indicate that the final value of the interhelix separation (R) is relatively insensitive to the initial value of R and to the corresponding
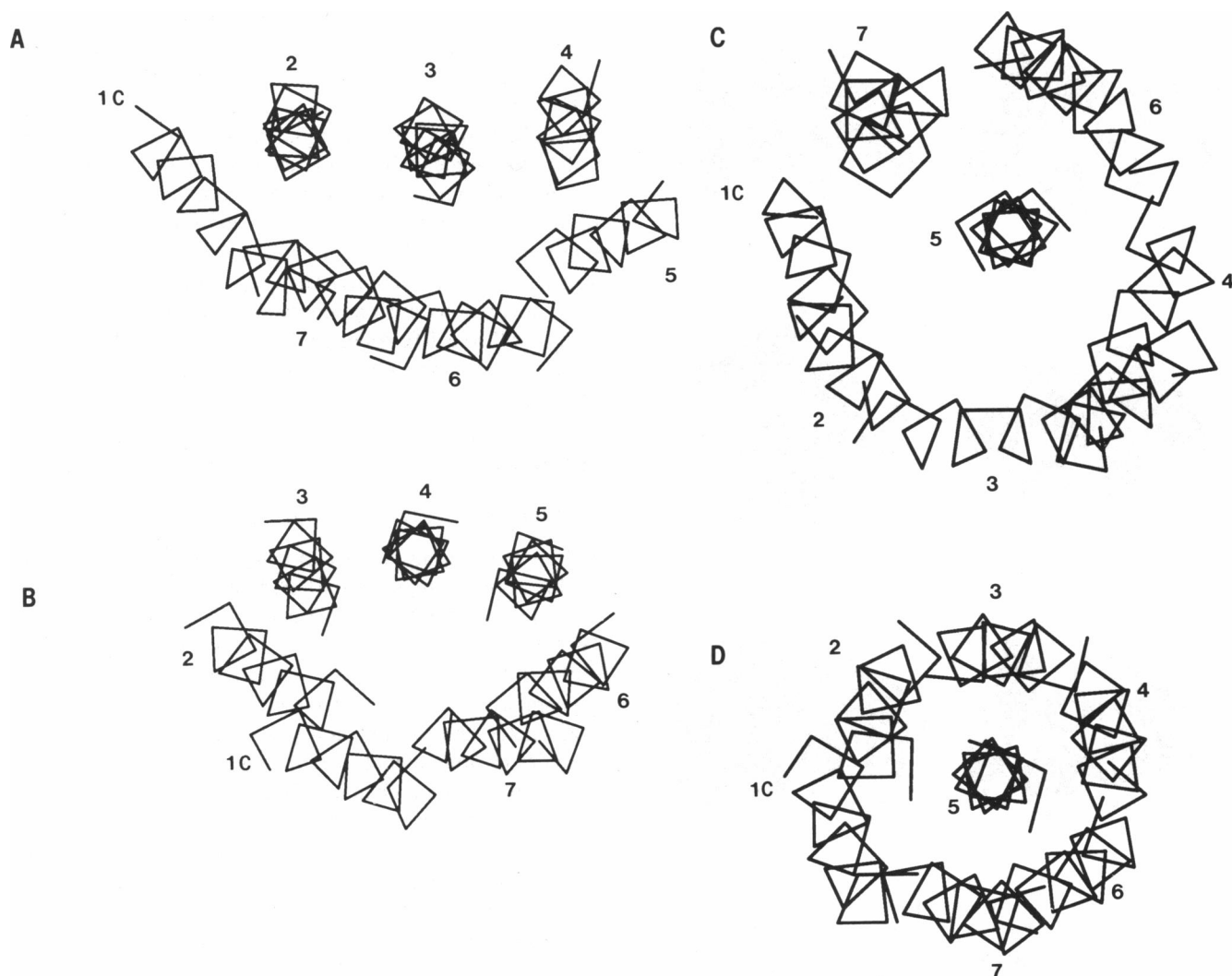
FIGURE 7 Comparison of experimentally determined and simulated 7TM bundle folds. The folds of (A) bacteriorhodopsin (Henderson et al., 1990) and of (B) ACH(4,4) both exhibit two layers (3+4) of TM helices. The folds of (C) the N-terminal domain of δ-endotoxin (Li et al., 1991) and of (D) ACS(4,1) both exhibit a central helix surrounded by a bundle of six helices. The positions of the seven helices and of the C terminus of helix 1 are labeled.

value of d_{TARGET} used in interhelix restraints (J. Breed and M. S. P. Sansom, unpublished data). With respect to the $C\alpha$ template helix geometry, studies on parallel dimers of hydrophobic helices show that despite using identical $C\alpha$-templates (corresponding to ideal α-helices), distinct (ϕ, ψ) values were obtained for Leu_{20} and for Aib_{20} helices, in agreement with a number of theoretical and experimental studies (Breed et al., 1995).

The main limitation of our implementation of SA/MD is that MD simulations are performed in vacuo, without either an explicit bilayer model or water molecules. However, interhelical distance restraints mimic a bilayer in maintaining the helices in an approximately (anti)parallel orientation. Furthermore, the surfaces of TM helices exposed to lipid exhibit high sequence variability, and so it is unlikely that specific interactions between amino acid side chains and lipid fatty acyl chains influence helix bundle formation. Ala_{20} helices are entirely hydrophobic, and electrostatic interactions do not appear to play a major role in bundle stabili-

zation. Consequently, the omission of water molecules may not have a major impact on the results of the simulations, other than on Gly_N loop conformations. Overall, such considerations suggest that in vacuo simulations provide a satisfactory first approximation to 7TM bundle formation within a bilayer.

Comparisons with other modeling studies

Relevant modeling studies may be divided into (a) analysis of the interactions of poly-Ala and related simple hydrophobic helices, and (b) simulations of structures for 7TM proteins. The former permits an evaluation of the success of SA/MD in modeling (anti)parallel helix bundles, whereas the latter investigations provide comparisons with 7TM bundle models arrived at by alternative approaches.

There are several studies concerning interactions in simple α-helical dimers. Chou et al. (1983) used energy minimization from multiple starting positions to model dimers of con-
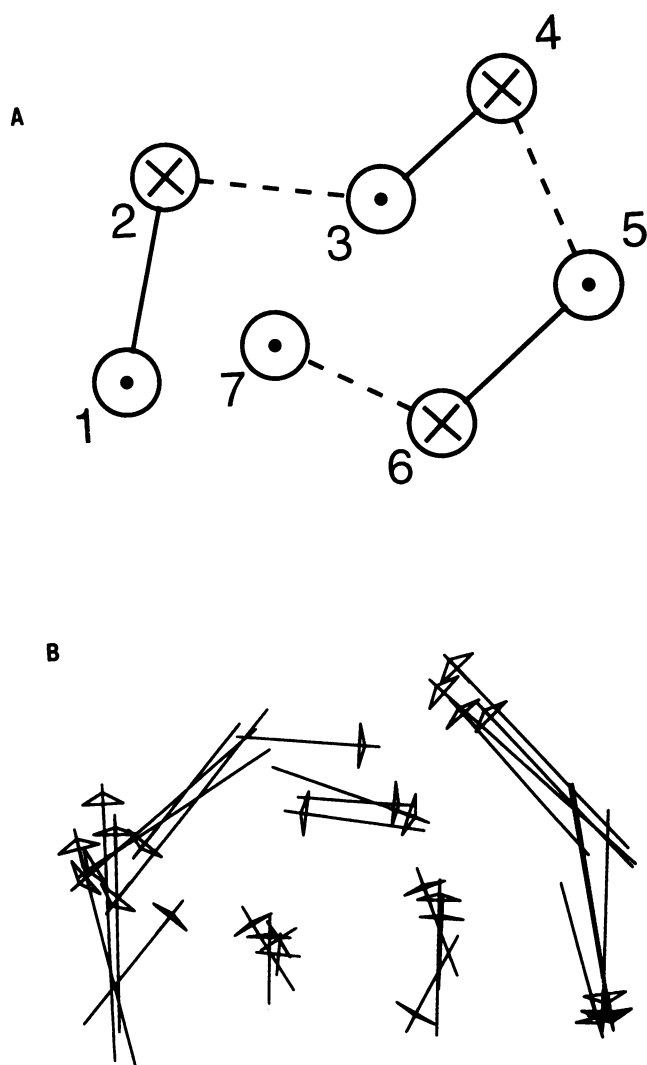
FIGURE 8 The conserved helix packing mode observed in ensembles ABS, AG5BH, AG5ZH, and AG10BH, compared with the two-dimensional projection structure of rhodopsin. The rhodopsin projection structure is shown schematically in A. The positions of the helices are derived from the positions of the peaks in the projection structure (Schertler et al., 1993). The assignment of the helices is based on the proposals of Baldwin (1993) and Donnelly and Findlay (1994). (B) Helix axis vectors for structures ABS-(1,2), AG5BH(1,1), AG5ZH(1,4), and AG10BH(3,3) superimposed. Helix 1 is at the bottom left-hand corner of the diagram.

formationally rigid Ala_{10} helices. The three most stable structures had helix crossing angles of $\Omega = -155°$, $+172°$ and $+150°$ (in order of decreasing stability). For the most stable ($\Omega = -155°$) dimer, $R = 7.6$ Å. Similar results were obtained for a heterodimer (Ala_{10}:Leu_{10}), for which $\Omega = -170°C$ and $+170°$ for the two most stable dimers (Chou et al., 1984). Thus, the most stable structures have $\Omega \approx -160°$, corresponding to Class 3-4 ridges-in-grooves helix packing. This corresponds closely to the Ala_{20} dimers generated via SA/MD, for which the ensemble average $\Omega \approx -175°$, but for which the most stable structures had $\Omega \approx -165°$ and $R \approx 7.8$ Å. The differences in geometry of the most stable dimers from the two studies may reflect differ-

ences in α-helix parameters: in Chou et al. (1983), (ϕ,ψ) was fixed at $(-57°, -47°)$, whereas for the SA/MD-generated dimers $(\phi,\psi) \approx (-65°, -40°)$. Broadly similar results were obtained for Ala_{14} dimers in energy minimization studies by Furois-Corbin and Pullman (1986), for which $\Omega \approx -166°$ and $R = 7.9$ Å. Overall, the most stable dimers from SA/MD are in good agreement with those from energy minimization. However, SA/MD suggests that a broad range of Ω values, centered about $\Omega \approx -175°$, are possible without large changes in potential energy. The difference in potential energy between the most stable dimers and the corresponding ensemble averages is only -5 to -10 kcal/mol.

Poly-Ala four helix bundles, made up of four 12-residue α-helices separated by three flexible 10-residue loops, have been modeled using energy minimization (Carlacci and Chou, 1990). The resultant bundle had $\Omega_{AP} \approx -163°$ and $R = 7.7$ Å. Comparison with a model without loops (Chou et al., 1988) suggested that the loops did not perturb helix packing within the bundle. However, calculations on both poly-Ala bundles (Carlacci and Chou, 1990) and on x-ray structures of four helix proteins (Chou and Zheng, 1992; Chou et al., 1992) suggested that the interaction energy between the helices and the loops was about twice the interhelix interaction energy. This agrees with the results in the current study, for which $\Delta E_{HL} \sim 2.5 \Delta E_{HH}$. In both studies, the helix-loop interaction is predominantly electrostatic in origin, presumably reflecting the formation of loop-helix H-bonds. Because neither study included explicit solvation, it is possible that the helix-loop interaction energy has been somewhat overestimated, but this interaction is still likely to be of importance in the net stabilization of 7TM bundles. However, our results suggest that such helix-loop interactions do not seem to perturb the geometry of the most stable helix bundles.

Furois-Corbin and Pullman (1986b) used energy minimization to generate (anti)parallel bundles containing from 3 to 7 Ala_{14} helices. Their 7-helix bundle was derived from an RH-circle template and had a distorted heptagonal structure reminiscent of BR. Helix crossing angles were not provided, but examination of the published structure suggests values of $\Omega_{AP} \sim -170°$. Thus, the (anti)parallel bundles generated in our study are broadly consistent with those in earlier, energy minimization-based, investigations. An advance in the current study is that a wider range of stable 7TM-packing geometries has been identified.

A valuable comparison may be made between 7TM bundles generated by SA/MD and a simulation of a poly-Ile 7TM bundle, including interhelix loops (Jähnig and Edhölm, 1992). The resultant poly-Ile bundle did not exhibit BR-like helix packing. However, one should note that the β-branched side chains of Ile may prevent efficient ridges-in-grooves packing of helices, as shown in an SA/MD study of parallel helix dimers and bundles (Kerr et al., 1994).

Several investigators have modeled 7TM proteins, including BR and various GPCRs (reviewed by Donnelly and Findlay, 1994). Jähnig and Edhölm (1992) ran 25 ps MD simulations in the presence of a bilayer-like potential

TABLE 9   Secondary structure of Gly_N loops

Ensemble	$\%\alpha$	$\%\beta$-Strand	$\%\beta$-Bulge	$\%3$-Turn	$\%4$-Turn	$\%5$-Turn	$\%$Random coil
Dimers							
AG5A	15	0	0	22	7	14	42
AG10A	11	6	1	14	5	20	44
7TM bundles							
AG5BH	21	1	1	18	4	13	42
AG5BS	23	1	2	16	4	17	37
AG5ZH	20	3	3	14	3	11	46
AG10BH	12	7	4	16	5	12	44

Note: For each ensemble, the percentage of the glycine residues adopting a particular secondary structure is given.

TABLE 10   Energetic analysis of helix-loop interactions

Ensemble	$\Delta E_{HL,TOT}$ (kcal/mol)	$E_{HL,VDW}$ (kcal/mol)	$E_{HL,ES}$ (kcal/mol)
Dimers			
AG5A	-57 (± 6)	-11 (± 4)	-48 (± 5)
AG10A	-66 (± 11)	-15 (± 4)	-52 (± 7)
7TM Bundles			
AG5BH	-359 (± 18)	-85 (± 8)	-283 (± 13)
AG5BS	-370 (± 16)	-88 (± 9)	-291 (± 15)
AG5ZZ	-367 (± 19)	-91 (± 12)	-285 (± 18)
AG10BH	-461 (± 29)	-107 (± 13)	-369 (± 18)

ΔE_{HL} is the mean helix-loop interaction energy for an ensemble. The overall interaction energy (TOT) and its van der Waals (VDW) and electrostatic (ES) components are given.

(Edholm and Jähnig, 1988) to model TM helix packing within BR. Interhelix loops between the BR helices were included in these simulations. Starting with the seven helices arranged in an LH-circle resulted in some compression of the circular bundle, but a BR-like packing was not achieved. Starting with a BR-derived template for the helices resulted in final helix tilt angles (and, hence, crossing angles) close to those in the experimental structure. This study reveals that once an approximate packing mode is achieved, refinement may be possible via realistic MD simulations. This is important in the context of the suggestion in the current study that SA/MD can be used to obtain approximate packing modes.

Chou et al. (1992) used simulated annealing in helix orientation and side-chain torsion angle space, starting with the EM-derived BR coordinates, to model possible conformational changes after photoisomerization of retinal. This provides an alternative to SA/MD for exploring a wide range of conformational space. It would be of considerable interest to compare such a Monte Carlo approach with that described here for packing simple hydrophobic helices in 7TM bundles.

The most promising studies of GPCRs have used homology modeling. As discussed by Donnelly and Findlay (1994), it is rather ambitious to apply a de novo approach to model ligand binding by GPCRs. A pioneering study by Hibert et al. (1991) used a BR template and energy minimization to model a number of GPCRs and to define ligand binding sites. More recently, Baldwin (1993) has analyzed 204 GPCR sequences in the context of the Rh projection structure. Consideration of minimum interhelix loop lengths suggested that sequence-

adjacent helices must also be spatially adjacent. Analysis of residue variability to define external faces of helices resulted in a tentative three-dimensional model, including assignment of the TM helices of GPCRs to the density peaks in the Rh projection structure. This has been elaborated by Donnelly and Findlay (1994) to generate a detailed model for Rh and other GPCRs. Packing of helices within this model resembles the Rh-like packing mode for seven Ala_{20} helices.

Implications of results

With respect to 7TM helix packing per se, our results suggest that there are a limited number of packing modes of (anti)-parallel helix bundles that are compatible with stereochemical (ridges-in-grooves) requirements. Perhaps this is to be expected, given the constraint of compact bundles and the need for helix crossing angles of $\Omega \approx +20°$ (for adjacent parallel helices) and $\Omega \approx -160°$ (for adjacent antiparallel helices). Observed stable structures suggest that core bundles of $6+1$ helices (δ-endoTx-like packing), $5+1$ helices (ACH-(4,1)), or $4+1$ helices (Rh-like packing) are formed, with remaining helices packed on the exterior of the core. This is a possible framework for modeling membrane proteins of unknown structure. Using SA/MD, a finite number of possible starting bundles could be generated for further refinement by extended MD simulations.

The results with respect to interhelix loops are also of significance. Conservation of the Rh-like packing mode between the AG5BH and AG5ZH ensembles suggests that although short interhelix loops require that sequence adjacent helices are spatially adjacent, they do not allow one to choose between alternative Cα templates that satisfy this criterion. Thus, for a membrane protein of unknown structure, additional experimental and theoretical information must be sought to select the correct template. Of course, Gly_N loops as used in this study are highly flexible. Inclusion of real sequences in loops might aid discrimination between alternative Cα templates for a given protein. However, recent x-ray studies of mutants of the ROP protein suggest that changes in the residues of α-α hairpin loops do not have a major effect on the structure of the 4-helix bundle (Vlassi et al., 1994).

It is instructive to compare the Rh-like packing mode with the model of Rh discussed by Baldwin (1993) and by Donnelly and Findlay (1994), and with proposals concerning

helix burial/exposure in GPCRs made by Zhang and Weinstein (1994). Referring to the helix assignment in Fig. 8 A, Baldwin concludes that helix 3 is the most buried, whereas Zhang and Weinstein conclude that both helices 3 and 7 are buried. Considering those structures that adopt the Rh-like packing mode (ACS(1,2), ABS(1,2), ABS(4,4), AG5BH(1,1), AG5BS(1,4), AG5ZH(4,4), AG5ZH(1,4), AG10BH(2,5), and AG10BH(3,3)), and taking into account the permutation of the helices within this packing mode in ACS(1,2) and the two AG5ZH structures, then in eight of the nine SA/MD structures helix 3 (or its permuted equivalent) is the most buried. Similarly, in eight of the nine structures helix 7 (or its equivalent) is the next most buried. Thus, the Rh-like packing mode obtained by simulations of Ala_{20} helices is in good agreement with predictions of the extent of helix exposure in GPCRs. This strengthens the suggestion that simple helix packing criteria provide clues as to possible $C\alpha$ template structures for integral membrane proteins.

Future directions

How might these studies be extended? One direction is to replace the distance restraints, used to impose (anti)parallel helix packing, by a bilayer potential similar to that developed by Edholm and Jähnig (1988) (also see Jähnig and Edhölm, 1992) alongside a compactness potential. Combining such an approach with solvation of extramembranous regions might improve modeling of the loops. The second direction is to apply SA/MD to real membrane proteins. This requires inclusion of information on exposed/buried faces of helices, probably in the form of empirical potential functions. With such inclusions, it is possible that restrained SA/MD provides approximate structures for simple integral membrane proteins.

REFERENCES

Baldwin, J. M. 1993. The probable arrangement of the helices in G protein-coupled receptors. *EMBO J.* 12:1693–1703.

Barlow, D. J., and J. M. Thornton. 1988. Helix geometry in proteins. *J. Mol. Biol.* 201:601–619.

Barsukov, I. L., D. E. Nolde, A. L. Lomize, and A. S. Arseniev. 1992. Three-dimensional structure of proteolytic fragment 163–231 of bacteriorhodopsin determined from nuclear magnetic resonance data in solution. *Eur. J. Biochem.* 206:665–672.

Breed, J., I. D. Kerr, R. Sankararamakrishnan, and M. S. P. Sansom. 1995. Packing interactions of Aib-containing helices: molecular modelling of parallel dimers of simple hydrophobic helices and of alamethicin. *Biopolymers.* In press.

Brooks, B. R., R. E. Bruccoleri, B. D. Olafson, D. J. States, S. Swaminathan, and M. Karplus. 1983. CHARMM: a program for macromolecular energy, minimisation, and dynamics calculations. *J. Comp. Chem.* 4:187–217.

Brünger, A. T. 1992. X-PLOR Version 3.1. A System for X-Ray Crystallography and NMR. Yale University Press, New Haven, CT.

Carlacci, L., and K. C. Chou. 1990a. Energetic approach to the folding of four α-helices connected sequentially. *Protein Eng.* 3:509–514.

Carlacci, L., and K. C. Chou. 1990b. Electrostatic interactions between loops and α-helices in four-helix bundle proteins. *Protein Eng.* 4:225–227.

Chothia, C. 1984. Principles that determine the structure of proteins. *Annu. Rev. Biochem.* 53:537–572.

Chothia, C., M. Levitt, and D. Richardson. 1981. Helix to helix packing in proteins. *J. Mol. Biol.* 145:215–250.

Chou, K. C., and C. Zheng. 1992. Strong electrostatic loop-helix interactions in bundle motif protein structures. *Biophys. J.* 63:682–688.

Chou, K. C., L. Carlacci, G. M. Maggiora, L. A. Parodi, and M. W. Schulz. 1992. An energy-based approach to packing the 7-helix bundle of bacteriorhodopsin. *Protein Sci.* 1:810–827.

Chou, K. C., G. M. Maggiora, G. Némethy, and H. A. Scheraga. 1988. Energetics of the structure of the four-α-helix bundle in proteins. *Proc. Natl. Acad. Sci. USA.* 85:4295–4299.

Chou, K. C., G. M. Maggiora, and H. A. Scheraga. 1992. Role of loop-helix interactions in stabilizing four-helix bundle proteins. *Proc. Natl. Acad. Sci. USA.* 89:7315–7319.

Chou, K. C., G. Némethy, and H. A. Scheraga. 1983. Energetic approach to the packing of α-helices. 1. Equivalent helices. *J. Phys. Chem.* 87:2869–2881.

Chou, K. C., G. Nemethy, and H. A. Scheraga. 1984. Energetic approach to the packing of α-helices. 2. General treatment of nonequivalent and nonregular helices. *J. Am. Chem. Soc.* 106:3161–3170.

Creighton, T. E. 1993. Proteins: Structures and Molecular Properties, 2nd ed. Freeman, New York.

Cronet, P., C. Sander, and G. Vriend. 1993. Modeling of transmembrane seven helix bundles. *Protein Eng.* 6:59–64.

Deisenhofer, J., O. Epp, K. Miki, R. Huber, and H. Michel. 1985. Structure of the protein subunits in the photosynthetic reaction centre of Rhodopseudomonas viridis at 3 Å resolution. *Nature.* 318:618–624.

Donnelly, D., and J. B. C. Findlay. 1994. Seven-helix receptors: structure and modelling. *Curr. Opin. Struct. Biol.* 4:582–589.

Donnelly, D., J. P. Overington, S. V. Ruffle, J. H. A. Nugent, and T. L. Blundell. 1993. Modelling α-helical transmembrane domains: the calculation and use of substitution tables for lipid-facing residues. *Protein Sci.* 2:55–70.

Edholm, O., and F. Jähnig. 1988. The structure of a membrane-spanning polypeptide studied by molecular dynamics. *Biophys. Chem.* 30:279–292.

Engelman, D. M., R. Henderson, A. D. McLachlan, and B. A. Wallace. 1980. Path of the polypeptide in bacteriorhodopsin. *Proc. Natl. Acad. Sci. USA.* 77:2023–2027.

Furois-Corbin, S., and A. Pullman. 1986a. Theoretical study of the packing of α-helices by energy minimization: effect of the length of the helices on the packing energy and on the optimal configuration of a pair. *Chem. Phys. Lett.* 123:305–310.

Furois-Corbin, S., and A. Pullman. 1986b. Theoretical study of the packing of α-helices of poly(L-alanine) into transmembrane bundles. *Biochim. Biophys. Acta.* 860:165–177.

Henderson, R., J. M. Baldwin, T. A. Ceska, F. Zemlin, E. Beckmann, and K. H. Downing. 1990. Model for the structure of bacteriorhodopsin based on high-resolution electron cryo-microscopy. *J. Mol. Biol.* 213:899–929.

Hibert, M. F., S. Trumpp-Kallmeyer, A. Bruinvels, and J. Hoflack. 1991. Three-dimensional models of neurotransmitter G-binding protein-coupled receptors. *Mol. Pharmacol.* 40:8–15.

Higgins, C. F. 1993. The multidrug resistance P-glycoprotein. *Curr. Opin. Cell Biol.* 5:684–687.

Hol, W. G. L., L. M. Halie, and C. Sander. 1981. Dipoles of the α-helix and β-sheet: their role in protein folding. *Nature.* 294:532–536.

Jähnig, F., and O. Edhölm. 1992. Modelling of the structure of bacteriorhodopsin: a molecular dynamics study. *J. Mol. Biol.* 226:837–850.

Jones, D. T., W. R. Taylor, and J. M. Thornton. 1994. A model recognition approach to the prediction of all-helical membrane protein structure and topology. *Biochemistry.* 33:3038–3049.

Kahn, T. Wa. E., and D. M. Engelman 1992. Bacteriorhodopsin can be refolded from two independently stable transmembrane helices and the complementary five-helix fragment. *Biochemistry.* 31:6144–6151.

Kerr, I. D., R. Sankararamakrishnan, O. S. Smart, and M. S. P. Sansom. 1994. Parallel helix bundles and ion channels: molecular modeling via simulated annealing and restrained molecular dynamics. *Biophys. J.* 67: 1501–1515.

Kraulis, P. J. 1991. MOLSCRIPT: a program to produce both detailed and schematic plots of protein structures. *J. Appl. Cryst.* 24:946–950.

Kühlbrandt, W., D. N. F. Wang, and Y. Fujiyoshi. 1994. Atomic model of plant light harvesting complex by electron crystallography. *Nature.* 367: 614–621.

Lemmon, M. A., and D. M. Engelman. 1994. Specificity and promiscuity in membrane helix interactions. *Q. Rev. Biophys.* 27:157–218.

Lemmon, M. A., H. R. Treutlein, P. D. Adams, A. T. Brünger, and D. M. Engelman. 1994. A dimerisation motif for transmembrane a helices. *Struct. Biol.* 1:157–163.

Li, J., J. Carroll, and D. J. Ellar. 1991. Crystal structure of insecticidal δ endotoxin from *Bacillus thuringiensis* at 2.5 Å resolution. *Nature.* 353: 815–821.

Livingstone, C. D., P. G. Strange, and L. H. Naylor. 1992. Molecular modeling of D2-like dopamine receptors. *Biochem. J.* 287:277–282.

Lomize, A. L., K. V. Pervushkin, and A. S. Arseniev. 1992. Spatial structure of (34 65) bacteriorhodopsin polypeptide in SDS micelles determined from nuclear magnetic resonance data. *J. Biomol. NMR.* 2:361–372.

MaloneyHuss, K., and T. P. Lybrand. 1992. Three-dimensional structure for the β_2-adrenergic receptor protein based on computer modeling studies. *J. Mol. Biol.* 225:859–871.

Nilges, M., and A. T. Brünger. 1991. Automated modelling of coiled coils: application to the GCN4 dimerization region. *Protein Eng.* 4:649–659.

Nilges, M., and A. T. Brünger. 1993. Successful prediction of the coiled coil geometry of the GCN4 leucine zipper domain by simulated annealing: comparison to the x-ray structure. *Proteins Struct. Funct. Genet.* 15:133–146.

Persson, B., and P. Argos. 1994. Prediction of transmembrane segments utilizing multiple sequence alignments. *J. Mol. Biol.* 237:182–192.

Pervushin, K. V., and A. S. Arseniev. 1992. Three-dimensional structure of (1–36)bacteriorhodopsin in methanol-chloroform mixture and SDS micelles determined by 2D 1H-NMR spectroscopy. *FEBS Lett.* 308: 190–196.

Popot, J. L. 1993. Integral membrane protein structure: transmembrane a helices as autonomous folding domains. *Curr. Opin. Struct. Biol.* 3:532–540.

Popot, J. L., and D. M. Engelman. 1990. Membrane protein folding and oligomerisation: the two stage model. *Biochemistry.* 29: 4031–4037.

Reddy, B. V. B., and T. L. Blundell. 1993. Packing of secondary structure elements in proteins: analysis and prediction of inter-helix distances. *J. Mol. Biol.* 233:464–479.

Richardson, J. S., D. C. Getzoff, and D. C. Richardson. 1978. The β bulge: a common small unit of nonrepetitive protein structure. *Proc. Natl. Acad. Sci. USA.* 75:2574–2578.

Richardson, J. S., and D. C. Richardson. 1989. Principles and patterns of protein conformation. *In* Prediction of Protein Structure and the Principles of Protein Conformation. G. D. Fasman, editor. Plenum Publishing Corp., New York. 1–98.

Sansom, M. S. P. 1991. The biophysics of peptide models of ion channels. *Prog. Biophys. Mol. Biol.* 55:139–236.

Sansom, M. S. P. 1993. Structure and function of channel-forming peptaibols. *Q. Rev. Biophys.* 26:365–421.

Schertler, G. F. X., C. Villa, and R. Henderson. 1993. Projection structure of rhodopsin. *Nature.* 362:770–772.

Sibanda, B. L., T. L. Blundell, and J. M. Thornton. 1989. Conformation of beta-hairpins in protein structures: a systematic classification with applications to modelling by homology, electron density fitting and protein engineering. *J. Mol. Biol.* 206:759–777.

Sylte, I., O. Edvarsen, and S. G. Dahl. 1993. Molecular dynamics of the 5-HT1a receptor and ligands. *Protein Eng.* 6:691–700.

Taylor, W. R., D. T. Jones, and N. M. Green. 1994. A method for α-helical integral membrane protein fold prediction *Proteins Struct. Funct. Genet.* 18:281–294.

Treutlein, H. R., M. A. Lemmon, D. M. Engelman, and A. T. Brunger. 1992. The glycophorin A transmembrane domain dimer: sequence specific propensity for a right handed supercoil of helices. *Biochemistry.* 31: 12726–12733.

Tuffery, P., C. Etchebest, J. L. Popot, and R. Lavery. 1994. Prediction of the positioning of the seven transmembrane helices in bacteriorhodopsin: a molecular simulation study. *J. Mol. Biol.* 236:1105–1122.

Unger, V. M., and G. F. X. Schertler. 1994. Three-dimensional structure of bovine rhodopsin at 9A. *Biophys. J.* 66:46a. (Abstr.)

Vlassi, M., C. Steif, P. Weber, D. Tsernoglou, K. S. Wilson, H. J. Hinz, and M. Kokkinidis. 1994. Restored heptad pattern continuity does not alter the folding of a four-α-helix bundle. *Nature Struct. Biol.* 1:706–716.

von Heijne, G. V. 1992. Membrane protein structure prediction: hydrophobicity analysis and the positive inside rule. *J. Mol. Biol.* 225:487–494.

Watson, S., and S. Arkinstall. 1994. The G-Protein Linked Receptor Facts Book. Academic Press, London.

Zhang, D., and H. Weinstein. 1994. Polarity conserved positions in transmembrane domains of G-protein coupled receptors and bacteriorhodopsin. *FEBS Lett.* 337:207–212.